Acta Materialia 267 (2024) 119716

Contents lists available at ScienceDirect

Acta Materialia

journal homepage: www.elsevier.com/locate/actamat

Crystal growth kinetics in BaS semiconductor: Molecular dynamics simulation and theoretical calculations

Leila Separdar [a,*], José Pedro Rino [a], Edgar Dutra Zanotto [b]

[a] Department of Physics, Federal University of São Carlos, Via Washington Luíz, km. 235, São Carlos, SP 13.565-905, Brazil
[b] Department of Materials Engineering, Federal University of São Carlos, Via Washington Luíz, km. 235, São Carlos, SP 13.565-905, Brazil

ARTICLE INFO

Keywords:
Crystal growth
Molecular dynamics simulation
Kinetics of crystallization
Solid-liquid interface
Phase-Field model
Growth velocity
Screw dislocations

ABSTRACT

Understanding the liquid-solid phase transition mechanisms and dynamics is of boundless scientific significance, and holds enormous technological relevance in designing mono or polycrystalline materials with tailored microstructures and property combinations. However, the atomistic mechanisms controlling these processes, and their associated theoretical models, remain elusive for most materials. In this article, we employ molecular dynamics (MD) simulations to investigate the crystal growth kinetics of a barium sulfide (BaS) semiconductor, used here as a model substance for which a reliable interatomic potential is available. The crystal growth velocities, $v(T)$, were estimated within two temperature intervals: at shallow supercooling, where spontaneous nucleation could not be observed within the MD time scale, $v(T)$ data were obtained by the embedded-seed method, and at deep supercooling, where spontaneous nucleation was detectable, $v(T)$ were computed directly from brute-force atomistic simulations. Relevant properties of the material, including density, enthalpy, and the self-diffusion coefficients, were also determined as a function of temperature. The growth rate data were analyzed using three classical theoretical models. The results indicate that the diffusion-controlled model using the screw dislocation mechanism and the kinetic phase-field model accurately describe the MD-derived $v(T)$ at both shallow and deep supercooling levels. However, only the diffusion-controlled theory using screw dislocation growth successfully captures the $v(T)$ peak, as predicted by all crystal growth theories and observed in the simulations.

1. Introduction

The mechanisms and kinetics of first-order phase transformations are ubiquitous and critically important in physics, chemistry, and materials science. Knowledge about how crystals nucleate and grow in supercooled liquids is fundamental for developing strategies to control the nano- or microstructure of materials, thereby influencing their properties. This knowledge can also be used to either inhibit or promote crystallization as needed. Crystallization occurs as a result of a stochastic process, with critical nuclei emerging from a supercooled liquid (SCL), followed by their subsequent transformation into long-range order structures.

According to the Classical Nucleation Theory (CNT), each temperature below the melting point corresponds to a critical nucleus of a specific size [1]. Crystal nuclei form as a result of thermal fluctuations; however, at shallow and moderate supercoolings, capturing their critical size using molecular dynamics (MD) is challenging because of their relatively large size and slow kinetics. In such cases, the embedded-seed method (ESM) [2,3] can be particularly helpful. This method circumvents the laborious process of spontaneous nucleation by artificially embedding a crystalline nucleus, or seed, into the parent liquid. The ESM has been employed for various purposes, such as determining the solid/liquid interfacial free energy [2,4], the crystal nucleation barrier [5,6], the relationship between critical nucleus size and temperature [4,7], condensation, the impact of seed shape [8–10], and crystal nucleation rates [11,12].

Regarding crystal growth, which is the main objective of this work, most previous studies to date have explored the movement of an idealized planar solid/liquid interface [7,13–17]; however, only a few of them have investigated the crystal growth kinetics using the ESM through MD simulations. For example, Bording et al. [3] studied the velocity of the crystalline/amorphous boundary as a function of nucleus size in a germanium model and determined the critical nucleus size at a deep supercooling. Mattoni et al. [18] studied the growth of embedded

* Corresponding author.
E-mail address: separdar.leila@gmail.com (L. Separdar).

https://doi.org/10.1016/j.actamat.2024.119716
Received 1 August 2023; Received in revised form 23 January 2024; Accepted 29 January 2024
Available online 3 February 2024

silicon crystallites, and showed that the growth of cylindrical grains in covalent materials is nonuniform. Zhou et al. [19] investigated the effect of the initial stress introduced by an artificially embedded seed on the crystallization process of aluminum. Recently, our research group has employed the ESM to determine the crystal growth rates in ZnSe [20] and analyzed the MD-derived growth velocities using two well-known theoretical growth models, which will be discussed later.

At deep supercooling, where the size of the critical nucleus becomes nanometric and the homogenous nucleation rates become significant, spontaneous nucleation (SpN) can be detected within the MD time scales for certain systems. However, not all model systems show SpN within the simulation time frame. Barium sulfide (BaS) is among those model systems showing SpN, thus providing an excellent opportunity to derive crystal nucleation and growth velocities directly from the simulation. Moreover, a highly reliable potential has been developed for this substance by our research group [21]. For these reasons, we have chosen this specific system for our study. The aim is to test several theoretical models.

Regardless of how a liquid-solid phase transformation initiates (whether by ESM or SpN), the subsequent objective of kinetic studies is to determine the stability of the growing phase and its growth velocity as a function of temperature. In the context of crystal growth, two fundamental and interrelated questions arise: What is the mode of growth or mechanism, and what is the growth kinetics? As evidenced by experiments [22], one of the distinguishing characteristics of crystal growth dynamics in supercooled liquids is the presence of a maximum, which is located somewhere between the melting and glass transition temperatures. According to the classical models, this peak arises as a result of the competition between opposing thermodynamic and diffusion-related effects. In the classical view of solidification theory [23,24], for atomically rough interfaces, just below the melting point, where the difference between the crystal and liquid Gibbs free energy values is small, $\Delta G \ll k_B T$, the growth velocity changes linearly with changing the temperature and the kinetic coefficient k, is the proportionality constant defined by the linear relation,

$$v = k(\hat{n})\Delta T \tag{1}$$

between the interface velocity, v, and the interface undercooling, $\Delta T = T_m - T$, where T_m is the melting point and T is the actual interface temperature, which can be higher than the average temperature of the bulk liquid due to the release of latent heat. The crystallization rate and hence $k(\hat{n})$ depend on the direction $\hat{n}$ normal to the interface with respect to a fixed set of crystal axes. Both the magnitude and anisotropy of k have a crucial influence on solidification. However, at significant undercooling levels (and corresponding high driving forces), nonlinearity emerges in the velocity-temperature behavior because of the decreasing diffusion coefficient, and k is not a single proportionality constant between v and ΔT, it depends on temperature and relates the growth velocity to a thermodynamic term $[1 - exp(-|\Delta G|/k_B T)]$, as shown below [25]

$$v(T) = k(T)[1 - exp(-|\Delta G|/k_B T)]. \tag{2}$$

As a result, a maximum is observed in the velocity *vs.* temperature curve. The linear relation is valid only when $\Delta G \ll k_B T$, where planar surface approximation gives a valid description of the kinetics of the solid/liquid interface motion. Because of experimentally attainable large driving forces and high growth velocities at deep supercoolings, care must be taken when using such approximation to analyze the crystallization dynamics.

Various theories have been developed to describe the crystal growth mechanism and kinetic processes occurring at solid/liquid interfaces. In this work, we aim to test three of the most well-known models, which are summarized below:

1) The Diffusion-Limited Theory (DLT) was proposed long ago by Wilson and Frenkel [26,27]. In the DLT, particle mobility controls the addition rate of atoms to a growing crystal, and the kinetic coefficient exhibits a strong temperature dependence, $k_{DLT}(T) \propto D(T)$, where $D(T)$ is an effective diffusion coefficient at the crystal/SCL interface. This model refers to a thermally activated process. The rearrangement of the local liquid structure, such as the reorientation of large organic molecules, and the breaking and rearrangement of bonds in network glasses are necessary for an atom to move and join the crystal. Consequently, there exists a kinetic barrier to crystallization [14]. This model has been previously applied to different materials with varying success. For instance, the maximum growth velocities calculated using this model agree well with those obtained experimentally for silicate glasses [28]. The DLT model with the normal growth mode described the experimental growth rate data well over a wide undercooling range ($T_g < T < T_m$) of silica [29], and growth rates obtained by computer simulations in fcc metals such as Ag, Pt, Ni, and Cu, as well as in bcc metals such as Fe, Mo, V, and Ta [15,30]. This was also true for a wide range of temperatures in metal alloys, including ZrCu and NiAl [31], and NiTi [32]. However, the DLT model failed to accurately describe the growth rates of these metals below their glass transition temperatures. It also either underestimated or overestimated the growth rates of other pure elements obtained by simulations [15].
2) The second model is the Collision-Limited Theory (CLT), which was proposed by Broughton, Gilmer, and Jackson to interpret crystallization rates measured by MD simulations in the Lennard-Jones system [33]. In this model, the attachment of particles to the crystal nucleus and the ordering kinetics are controlled by the average thermal velocity of the particles, $k_{BGJ}(T) \propto \sqrt{T}$ and there is no energy barrier to particle motion across the liquid/crystal interface, and thus no need to rearrange the liquid local structure for crystallization. This diffusionless growth model has also successfully explained the experimentally measured crystal growth velocities in various systems. These include colloidal systems at deep supercooling [34] and silver at shallow supercooling [22]. The model also aligns with results from simple metals such as Na [35], Co [36] and Ag, Au, Cu, and Ni at shallow supercoolings – specifically just before their growth velocities reach their maximum values [37], and also applies to certain alloys [38,39]. However, this model has failed to accurately describe the growth velocities in multicomponent alloys [31, 40–42].
3) The third model is known as the Phase-Field (PF) model. In this approach, the solid/liquid interface is treated as a region with a finite width, showing a gradual variation of physical quantities, which are referred to as phase fields or order parameters [43]. In this model, the phase-field parameter, φ, and its gradient flow, $\frac{\partial \varphi}{\partial t}$, are introduced as independent thermodynamic variables in the Gibbs free energy potential, $G\left(T, C, \varphi, \frac{\partial \varphi}{\partial t}\right)$, where C is the solute concentration. Traditional PF models, based on the hypothesis of local thermodynamic equilibrium (where $\frac{\partial \varphi}{\partial t} = 0$), only predict the linear behavior of crystal growth velocity, $v(T)$, at a small driving force, i.e., $v \propto \Delta G$. This prediction has been successfully tested by atomistic simulations at relatively low interface velocities [44]. The physical background and a detailed thermodynamical derivation of the phase-field equations can be found in review articles, such as in Ref. [43]. Galenko et al. [45] have recently reformulated the phase-field equations to consider deviations from local equilibrium in crystal growth kinetics [46–48]. They have successfully tested the PF model to describe experimental growth velocities in the Cu-Zr(-Ni) alloy [49] and on MD-derived data for rapidly growing crystals of $Al_{50}Ni_{50}$ [46], Fe [48], and Cr [50]. The model also successfully described common aspects of the solid/liquid interface kinetics, such as nonlinearity behavior in the temperature dependence of growth rates over a wide temperature range. The DLT of Wilson and Frenkel was not able to

Table 1
Set of pair potential parameters used in the MD simulation of BaS.

	Ba	S	
$Z(e)$	1.615972	− 1.615972	
σ (A°)	1.286	1.914	
$\alpha(A^{\circ 3})$	2.5	5.9	
	Ba-Ba	Ba-S	S-S
$A(J)$	0.8441×10^{-19}	0.8441×10^{-19}	0.8441×10^{-19}
$W(JA^{\circ 6})$	0	4.9303×10^{-18}	0
η	11	9	7

quantitively describe $v(T)$ in these materials. However, in a further test, this model failed to explain the temperature dependence of growth velocities in Si [50].

Hence, a question remains elusive: which model, if any, accurately describes the crystal growth rates for different substances across a wide temperature range? This problem certainly demands further study.

In a previous work, we obtained the nucleation rates of BaS at shallow supercooling using the ESM and the CNT [51]. We extrapolated the data to deep supercoolings and successfully compared the CNT predictions with the nucleation rates obtained directly from SpN. In this study, we aim to move one step further and analyze the crystal growth mechanism and dynamics in this same material by testing the predictive power of the aforementioned theoretical models using physical properties and kinetic data obtained directly from MD simulations. BaS was selected as a model material for three main reasons: (i) it is an important semiconductor with applications from ceramics and flame retardants to luminous paints and additives, and recent research has shown its potential technological applications in electrical and optical devices [52]; (ii) a reliable potential has been developed for its simulation [21]; (iii) as previously mentioned, BaS crystalizes spontaneously at deep supercooling and growth velocities can be obtained directly from brute force MD simulations.

The paper is organized as follows: In Section 2, we present the details of the simulation techniques, the pair potential, and the simulation results. Section 3 is devoted to the MD results and comparing the theoretical models. Finally, in Section 4, we sum up the paper and present a discussion and conclusions.

2. MD simulations and results

A reliable pair potential proposed by Rino [21] was used for the simulation of BaS. This potential consists of 4 terms: steric repulsion, Coulomb interactions due to charge transfer between ions, charge-induced dipole attractions due to the electronic polarizability of anions, and the Van der Waals attraction. The mathematical expression for this potential is given by

$$V(r) = \sum_{i<j=1}^{N} V_{ij}(r_{ij}) \tag{3}$$

$$V_{ij}^{(2)}(r) = A\left(\frac{\sigma_i + \sigma_j}{r}\right)^{\eta_{ij}} + \frac{Z_i Z_j}{r}.e^{-r/\lambda} - \frac{\alpha_i Z_j^2 + \alpha_j Z_i^2}{2r^4}.e^{-r/\xi} - \frac{W_{ij}}{r^6} \tag{4}$$

where, σ_k is the ionic radius of each atom, A is the intensity of the steric repulsion, Z_k is the effective charge of the ions in units of electronic charge, α_k is the electronic polarizability, and W is the intensity of the Van der Waals attraction. η, $\lambda = 4.5A^{\circ}$, and $\xi = 3.0A^{\circ}$ stand for the exponents of the steric repulsion, the screening lengths for the Coulomb, and charge-induced dipole interactions, respectively. The potential is truncated at $r = r_c = 7.0A^{\circ}$ and shifted to zero for $r > r_c$ to ensure its continuity, as well as that of its first derivative, at r_c. All the parameters of this pair potential are given in Table 1. The Nosé-Hoover thermostat and barostat with coupling parameter 0.01 and 0.5 were used to control the temperature and pressure (see Appendix A for details about tuning the thermostat relaxation time). Using this potential, the melting point of BaS was determined by the solid/liquid coexistence method which is $T_m = 2450 \pm 20$ K [21]. All simulations were performed by the LAMMPS software [53] in NpT ensemble with a periodic boundary condition at zero pressure.

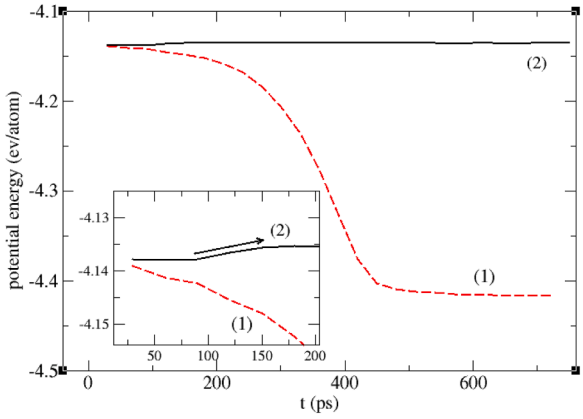

Fig. 1. Time evolution of the potential energy of the supercooled liquid containing a crystalline seed with radius 17A° at $T_{on} = 2114$ K. In curve (1) the potential energy decreases sharply demonstrating that the seed grows, whereas in curve (2) the $U(t)$ remains approximately constant after a small increase at a short time interval, which indicates seed dissolution. The inset shows the time interval at which the $U(t)$ increases in curve (2).

2.1. Growth rates obtained from the ESM at shallow supercooling

Our procedure for obtaining the growth rates using the ESM relies on finding the onset temperature of seed growth, T_{on}, the temperature at which the seed starts to grow. To find this temperature, initially a system containing 64,000 particles arranged in a perfect rock-salt structure and well equilibrated at 50 K at zero pressure. Then the thermalized crystal was heated to 1500K and two regions were defined inside the simulation box: (1) the crystalline zone, which was chosen as a spherical region of radii $r^* = 17$, 15, 13, and 11 A° and (2) a melting zone, which contains all atoms outside the spherical region. The crystal outside the spherical zone was melted by increasing the temperature up to $T = 3400$K well above the melting point, whereas the atoms in the crystal zone were kept fixed at their positions at $T = 1500$K. After equilibrating the liquid atoms at $T = 3400$K, the liquid atoms were cooled down from $T = 3400$K to 1500K at a cooling rate of 50 K/ps, while maintaining the seed atoms in their fixed positions at $T = 1500$K . During this cooling step, we saved data files at intervals of 200 time steps. These files contained information about the positions and velocities of all particles in the system, enabling the simulation to be restarted at any chosen temperature with 10K intervals (e.g., the restart files refer to $T = 3400$, 3390, 3380, etc.). In the next step, the restart files were used, and the constraints of the seed atoms were removed. The system (liquid + seed) was let to evolve by time at each specific temperature under zero pressure to assess whether the seed grew or dissolved. This was determined *via* the time evolution of the potential energy $U(t)$. A sharp decrease in potential energy indicates seed growth and the beginning of phase transition, whereas if $U(t)$ increases, this means that the crystal seed dissolved into the SCL. Fig. 1(a), shows $U(t)$ for two different configurations, both of them containing a seed with radius 17A°, corresponding to 784 atoms of a total 64,000 in the simulation box. In one of them the inserted seed dissolves (black line) and in the other one it grows (red dashed line). In the ESM method we do not expect a sharp increase in $U(t)$, because the radius of the inserted seed is small in comparison to the simulation box, hence, when the seed dissolves, it does not change the $U(t)$ significantly. Because the dissolution occurs in a short time interval, 100ps $< t <$ 150 ps, the plot of $U(t)$ for a longer time interval does not

Table 2
Seed growth onset temperatures (T_{on}), and average growth velocities $v(T)$, obtained from ESM and SpN.

r^*(A°)	17	15	13	11	Spontaneous nucleation		
T_{on} (K)	~ 2114	~ 2072	~ 2019	~ 1945	1700	1600	1400
$v(T)$ (A°/ps)	0.32	0.37	0.39	0.43	0.43	0.42	0.3

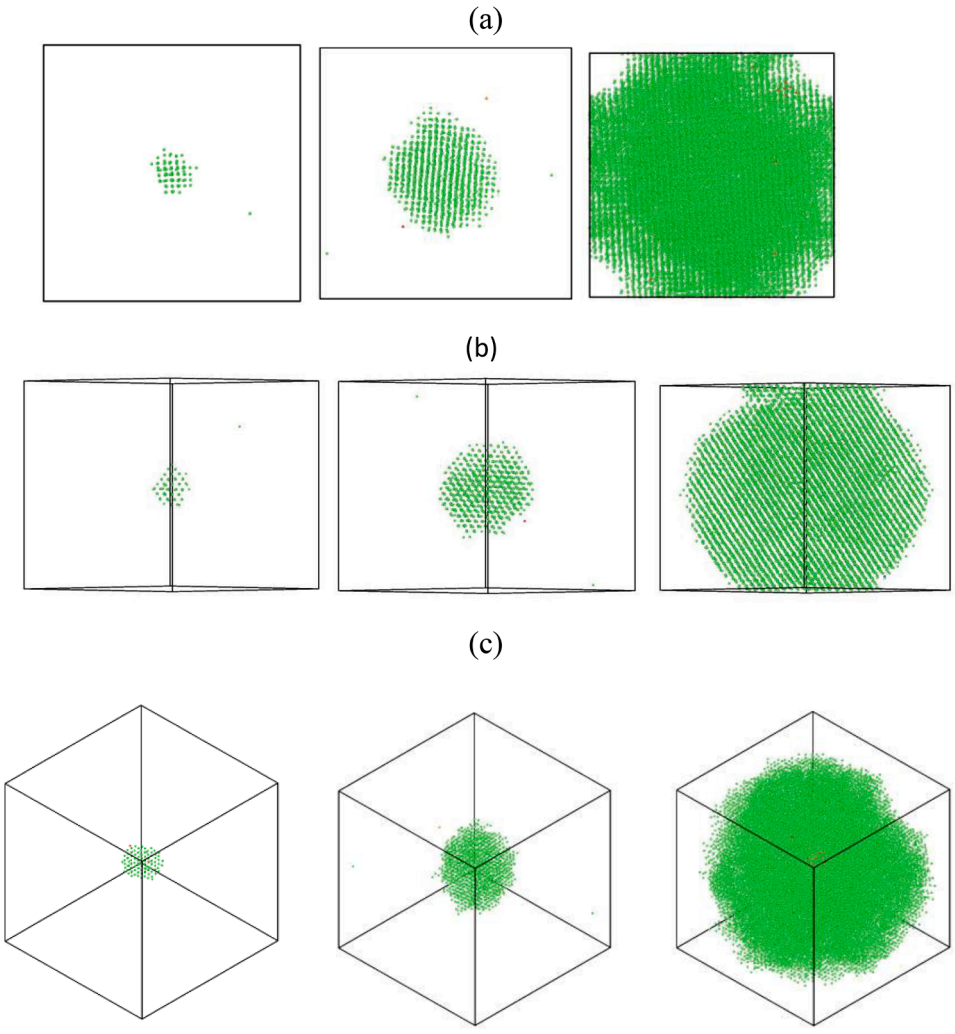

Fig. 2. Snapshots of the time evolution of the seed cross-section area with $r^* = 11$A° at $T_{on} = 1945$K in directions (a) [100], (b) [110] and (c) [111] at three times $= 0,\ 100,$ and 200 ps.

show that small change. In this way, we found a "candidate" for the onset temperature. After determining the possible onset temperature, because close to T_{on} the nucleus can grow or shrink stochastically, for better statistics, at some temperatures above and below T_{on}, we preformed 10 independent tests. The temperature at which the seed grew in more than half of the 10 experiments, and fully dissolved in the others, was selected as the definitive onset temperature. For $T < T_{on}$, the seed grew in all 10 independent configurations, whereas for $T > T_{on}$, it did not grow at all or grew in fewer than five configurations. This procedure was repeated for three other different seed sizes. Different techniques have been used for inserting a seed inside a supercooled liquid. For example, in one method a crystalline seed is inserted by replacing the atoms inside a sphere in the center of the simulation box, as some authors have done for water, Lennard–Jones, Silica, and NaCl. In this procedure, the seed/liquid interface acquires many unsuccessful configurations, and thus has a high potential energy. Hence, the interface must be equilibrated. In another method, which is called the persistent-embryo method [54], the seed is restrained from remelting by an external spring to constrain the embryo. As the embryo grows, the harmonic potential is gradually weakened and is completely removed. The procedure that we used in this work not only has the advantage that the liquid-solid interface produced has no artificial disorder but also decreases the effect of the difference between the density of the crystalline seed and the parent liquid. The estimated onset temperatures for four seed sizes are shown in Table 2. At T_{on}, for those configurations that the seed grows, we let the system evolve for a longer time until it thoroughly crystalized.

The crystal growth has been monitored from different directions. Fig. 2 depicts snapshots of the time evolution of the seed cross-section area with radius $r^* = 11$A° at $T_{on} = 1945$K in directions (a) [100], (b) [110] and (c) [111] at three times $= 0,\ 100,$ and 200 ps, showing that the seed conserves its spherical shape during growth, with unsignificant faceting, which is necessary for the formation of new layers on the previous spherical layer at each time step.

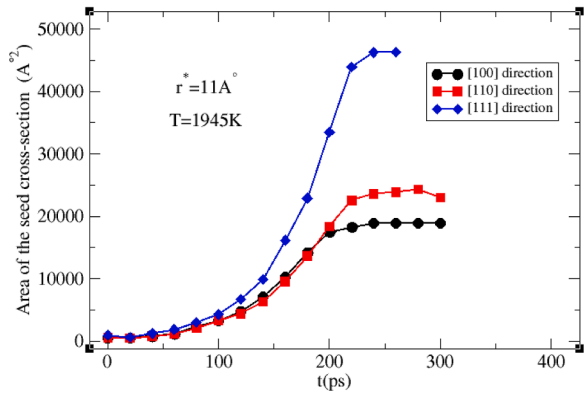

Fig. 3. Time evolution of the seed cross-section area in different crystallographic directions for the same selected configuration. The growth velocities are equal in the [100] and [110] directions but about three times slower than in the [111] direction.

In most materials, the crystallization velocity is dependent on the front orientation [20,31]. Using the Fiji software [55], we measured the cross-section area of the growing seed at selected intervals. These measurements are shown in Fig. 3 by solid lines + symbols in three directions [100], [110] and [111]. The growth rates in the [100] and [110] directions are the same, but about three times slower than in the [111] direction. The slopes in the [010], [001], [100], [101], and [011] directions, which are not shown in this figure, were also similar. These calculations show the crystallography direction dependence of crystal growth. The same growth behavior was observed in other configurations with varying seed sizes.

To find the growth velocities, solid-like particles in the seed environment were identified by calculating the Steinhardt bond-order parameter [56,57], $S_{ij} = \sum_{m=-6}^{m=+6} q_{6m}(i).q^*_{6m}(j)$, where $q_{6m}(i) = \frac{1}{N_b(i)} \sum_{j=1}^{N_b(i)} Y_{lm}(\vec{r}_{ij})$ is the Steinhardt parameter and q^*_{6m} is the complex conjugate of q_{6m}. In this equation, $Y_{lm}(\vec{r}_{ij})$ represents the spherical harmonics, $N_b(i)$ is the number of the nearest neighbors of atom i and $\vec{r}_{ij}$ is the vector connecting atom i with its neighbor j. If the value of the dot product was $q_6.q^*_6 > 0.5$, the particle-particle association was considered solid-like [58]. We tested the q_6 results using a set of different numbers of connections, $N_b(i)$, at one temperature to find the most appropriate number for crystallization cases. If a particle was involved in more than six solid-like associations, it was considered to be in the seed environment. This number agrees with the coordination number calculated from the area under the first peak of the radial distribution function [59], and is typical for the rock salt crystal structure. Fig. 4(a) shows the time evolution of the average number of solid-like atoms during the growth of inserted seed with radius $r^* = 11$ A° at its onset temperature, $T_{on} = 1945$K. The seed growth process shows a typical sigmoidal appearance, indicating that it evolves from an initial slow growth (time interval Δt_1), to rapid growth with constant rate (time interval Δt_2), and finally the growth process is ceased because of the finite size effect (time interval Δt_3). From $N(t)$, using the crystal number density at $T_{on} = 1945$ K and by assuming that the cluster conserves its spherical shape during all growth stages, we found the time dependency of the nucleus radius from the relation $r(t) = \left(\frac{3N(t)}{4\pi\rho_s}\right)^{1/3}$. Fig. 4 (b) shows the time evolution of the seed radius. A linear fit to data in the intermediate time interval, Δt_2, gives the nucleus growth velocity. The average growth velocity of the seed with $r^* = 11$ A° over five independent configurations was $v = r = 0.43 \pm 0.02$ A°/ps. This procedure was repeated for three other seed sizes and the estemiated velocies are reported in Table 2.

There are two ways to verify whether the growth velocities relate to the steady-state growth regime (where the slope of the $v(T)$ remains constant during the time interval Δt_2). First, we inserted seeds with $r > r^*$ at each T_{on} and, by repeating the same process, we calculated the $v(T)$ for larger seed sizes. In this way, we discovered that the average growth velocities are approximately equal to the growth velocity of the critical seed size. For example, seeds with radii $r = 13,\ 15,$ and 17 A° at $T_{on} =$ 1945K related to $r^* = 11$ A° grew with the average growth velocities $v = 0.46,\ 0.43,$ and 0.45 A°/ps, respectively. The second way is by simulation of a larger system. Fig. 5 shows the time evolution of solid-like atoms $N(t)$ for four different system sizes containing 17, 568, 32, 768, 64, 000, and 125, 000 atoms, all containing the same seed size of 17A°. As demonstrated in this figure, for the smallest system size, seed

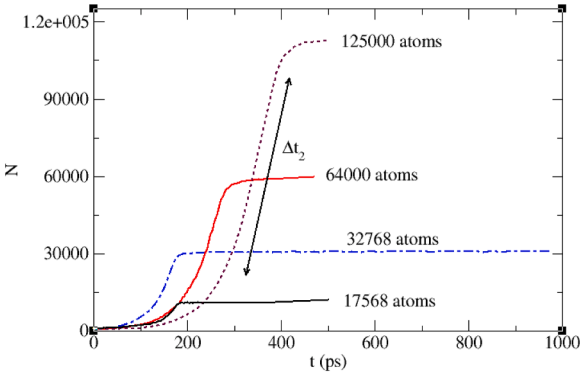

Fig. 5. Time evolution of solid-like atoms for four different system sizes all containing the same seed size of 17A°. For the smallest system size, seed growth is halted by its periodic image immediately after entering the steady-state growth regime (black solid line). Increasing the system size makes the steady-state stage of crystal growth related to time interval Δt_2 distinguishable from the two other stages.

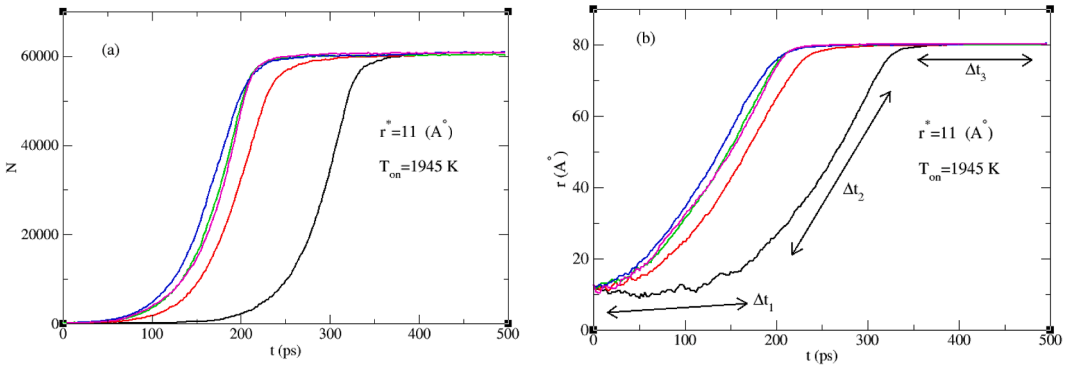

Fig. 4. (a) Time evolution of the number of solid-like atoms in the system containing a seed with initial radius $r^* = 11$ A° at its onset temperature $T_{on} = 1945$K; (b) time evolution of the radius of the seed calculated from $N(t)$ and the crystal density.

growth is halted by its periodic image immediately after entering the steady-state growth regime (black solid line). Doubling the system size from 17,568 to 32,768 atoms renders the steady-state stage of crystal growth distinguishable from the two other stages. However, for better statistics and more reliable results, we doubled this system size again to 64,000 atoms and then to 125,000 atoms. These changes did not alter the growth velocity. As it can be seen in Fig. 5, the slope of the system containing 125,000 atoms is the same as for the system containing 64,000 atoms. The radial growth velocity was determined by a linear fit to the data in this intermediate regime. This confirmed that the computed growth velocities had reached to their size-independent growth regime.

2.2. Spontaneous nucleation and crystal growth at deep supercoolings

In a previous work addressing nucleation kinetics, we showed that BaS spontaneously crystalizes at temperatures below $T = 1700$K [51]. To obtain the growth velocities directly from the simulations using spontaneous crystallization, we let the supercooled BaS, without inserting a seed, evolve for more than 1.5 ns at three temperatures: $T = 1700, 1600,$ and 1400K, and then counted the number of solid-like atoms *via* the Steinhardt bond-order parameter, as explained in Section 2.1. In spontaneous nucleation, more than one nucleus could form within the simulation box and, during the growth procedure, they could overlap to form unusually large crystalline clusters. In this case, the Radius versus Time plot would not be linear and show some noticeable kinks when the clusters overlapped. In our study, the growth velocity within the spontaneous nucleation region was obtained directly from the number of solid-like atoms, and then related to the one-dimensional growth *via* the number density relation $\rho_s = N(t)/V(t)$, where $V(t)$ is the time evolution of crystalline volume at each temperature. No kinks were observed in our plots. The results are reported in Table 2.

2.3. Growth rates of the seeds with a specific radius at $T < T_{on}$

To determine the temperature dependence of $v(T)$, using the seeding method, we applied another procedure, as used in some previous MD studies [19]. In this procedure, after identifying the onset temperature, a seed of the same size was introduced into a SCL at several temperatures lower than its onset temperature. The growth velocities were then determined at $T < T_{on}$. The difference between this procedure and that explained in Section 2.1 is that in the later the growth velocities of the seeds with different radii were determined at their corresponding onset temperatures, but here the growth rate of one given seed with a specific radius was obtained at $T < T_{on}$. We also applied this method and found the $v(T)$ for the radii of two seeds $r^* = 11$ and 17A°. The seed with radius $r = 17$A° and $T_{on} = 2114$K was inserted into the SCL at temperatures $T = 2000, 1950, 1900, 1850, 1800, 1700$K while the seed with radius $r = 11$ A° and $T_{on} = 1945$K was introduce into the SCL at temperatures $T = 1900, 1850, 1800, 1700$K. We used these set of data points to validate the theoretical fitting. With this procedure, we discovered that the growth rates of seeds with radii $r = 11$ and 17 A° at $T = 1700$K are equal to the one obtained from SpN. This finding further confirms that the calculated $v(T)$ values are associated with the size-independent growth regime. In Section 3, we briefly review three theoretical models introduced in Section 1, i.e., DLT, CLT and PF. Then the MD-derived growth velocities are fitted with their relevant formalism to find which model most accurately describes the growth kinetics throughout the temperature range.

3. The theoretical models and their predictions

In the kinetic theories of crystal growth, the race between two atomic fluxes at the solid/liquid interface one flux from the liquid to a crystal with rate v^+ and the second from a crystal to the liquid with rate v^- results in the non-zero interface velocity. The growth rate can be written in the form [60,61]:

$$v(T) = v^+ - v^- = k(T)[1 - exp(-|\Delta G|/k_B T)], \tag{5}$$

where, $k(T)$ is the rate at which atoms or molecules join the crystal, k_B is the Boltzmann constant, $\Delta G = G_{cry}(T) - G_{liq}(T)$ is the Gibbs free energy change, which is negative in solidification. For the analytical estimates, we express the thermodynamic driving force in its widely used form [25],

$$\Delta G = \Delta h_m \frac{(T_m - T)}{T_m} \tag{6}$$

where, Δh_m is the difference in the enthalpy of the crystal and liquid at the melting point (heat of melting). For BaS, this value is 0.296 $ev/atom$ [51]. At deep supercoolings, the thermodynamic factor, $[1 - exp(-|\Delta G|/k_B T)]$, approaches the unity, whereas the kinetic factor, $k(T)$, increasingly slows as the temperature drops. Determining this kinetic term is a necessary but challenging component to test growth theories. Based on the relationship between the thermodynamic and kinetic terms, different theoretical models have been proposed to describe the crystal growth mechanism and dynamics.

Since crystal growth kinetics in BaS were investigated up to an undercooling of $\Delta T = 1100$ K, a regime where temporal relaxation processes are known to occur, we investigated the potential influence of relaxation on growth dynamics. Eq. (5), used to model growth, does not account for relaxation effects. Therefore, we compared the characteristic times for growth with structural relaxation times across the studied undercooling range. Our analysis demonstrates that structural relaxation in BaS significantly precedes crystal growth (details in Appendix B). This finding indicates that SCL relaxation does not directly influence crystal growth rates in BaS in this temperature range.

3.1. Prediction of the Diffusion-Limited Theory (DLT)

The DLT, formulated by Wilson and Frenkel [26,27], relates the kinetic coefficient, $k(T)$, to a frequency of the order of the Debye frequency, times a Boltzmann factor, $\exp(-E_A/k_B T)$, where E_A is an activation energy associated with the mobility of the atoms or molecules across the liquid/crystal interface. Wilson associated this activation energy with the diffusion process in the liquid, which can be written as:

$$D(T) = D_0 \exp\left(-\frac{E_A}{T}\right) \tag{7}$$

Hence,

$$k^{DLT}(T) = \frac{fCLD(T)}{\lambda^2} \; where \begin{cases} f \approx constant \approx 1.0 \; Normal \; growth \; mode \\ f \cong \dfrac{(T_m - T)}{2\pi T_m} \; Screw \; Dislocation \; growth \; mode, \end{cases} \tag{8}$$

here λ is the jump distance or displacement during crystallization, which is proportional to the lattice parameter, L, and can be related to the position of the first peak in the radial distribution function and C is the rate of addition of layers per diffusion time after factoring the reverse process contribution to the dynamics. This unitless parameter C is obtained from fitting. The crystallographic dependence of growth velocity is reflected into the theory through the lattice parameter L. f is the density of preferred growth sites at the solid/SCL interface, and its value depends on the mode of growth. In the "Normal or Continuous" mode of growth, which is supposed to take place on atomically rough crystal interfaces, there is no difficulty in forming new layers, $f \approx constant \approx 1.0$, and independent of the undercooling. Whereas in the "Screw Dislocation" mode, the density of available growth sites depends on the number density of screw dislocations on the growing crystal surface, hence f depends on the undercooling [62]. In this case, $f << 1$ on the crystal surface, and is given approximately by the Uhlmann expression,

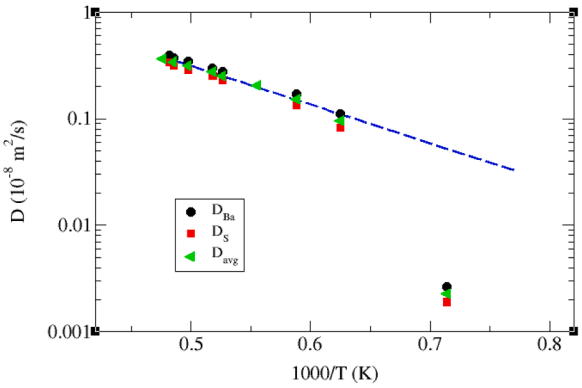

Fig. 6. Arrhenius plot of the simulated translational diffusion coefficient, $D(T)$, obtained from the mean squared displacements *via* the Einstein relation. The dashed line refers to a fit according to the Arrhenius expression (Eq. (7)) to the average diffusion coefficients. The data depart from the Arrhenius line for $T < 1650$ K, where the SCL crystallizes directly on the cooling path.

$f \cong \frac{(T_m - T)}{2\pi T_m}$ [63,64].

When the solid/SCL interface is defect-free, there is another mechanism, referred to as 2*D* or Secondary Surface Nucleated growth model [65], which will not be further discussed here because it is quite rare in inorganic materials, most of their crystals have surface defects.

To apply the DLT, we first obtained the diffusion coefficients, $D(T)$, using the mean-square displacements *via* the Einstein relation, $\langle r^2(t)\rangle = 6Dt$, for the two elements, Ba and S, in the 1400 K $< T <$ 2100K temperature range. The resulting diffusion coefficients were fitted using the Arrhenius Eq. (7), down to $T = 1700$K. The activation free energies were $E_A = 0.66$ eV for Ba and $E_A = 0.72$eV for S. The pre-exponential factors were $D_0 = 16.04$ A$^{\circ 2}$/ps for Ba and $D_0 = 19.6$A$^{\circ 2}$/ps for S. Fig. 6 shows the Arrhenius plot of the simulated translational diffusion coefficient, $D(T)$. The dashed line shows the fit to the average diffusion coefficient, $D_{avg} = (D_{Ba} + D_S)/2$, according to Eq. (7). A breakdown from Arrhenius behavior occurs below $T = 1650$K, where the SCL crystallizes immediately on the cooling path. This breakdown indicates "dynamic heterogeneity" within the system, which is indeed a characteristic property of fragile liquids. To determine the factor C, using Eqs. (5) and (8), we rescaled the growth velocity as

$$v(T)\lambda^2/fLD(T) = C[1 - exp(-\Delta G / k_B T)]. \quad (9)$$

substituting the values of v, $\lambda = 3.1$A$^{\circ}$(the position of the first peak of the radial distribution function of the Ba-S pairs), the D_{avg} at each temperature, and the ΔG from Eq. (6), we plotted $v(T)\lambda^2/LD(T)$ as a function of $[1 - exp(-\Delta G/k_B T)]$ for the Normal mode of growth, (see Fig. 7(a)). A linear relationship was observed, demonstrating that the expression presented in Eq. (9) had indeed successfully captured it. The values of C are 20.62, when only data obtained from the ESM are used, and 32.86, when all data points related to both ESM and SpN are used. Having attained the temperature dependence of D and C, we extrapolated the data toward deep supercooling, which is depicted by the red and green dashed lines in Fig. 7 (b), for each data set used for fitting. The same procedure was carried out for the DLT assuming a screw dislocation

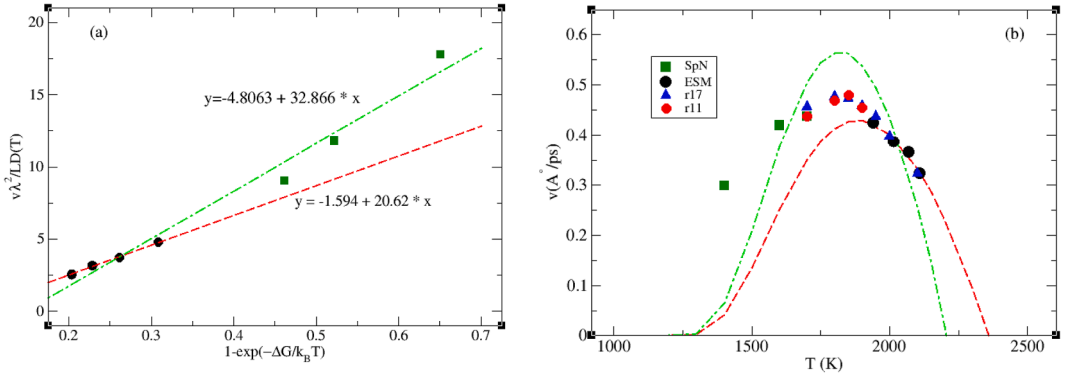

Fig. 7. (a) Reduced growth rates as described in the text (Eq. (9)) considering the "Normal" mode of growth, $f \approx constant \approx 1.0$. (b) Temperature dependence of the average crystal growth rate. In both figures, the black circles correspond to data obtained from the ESM at low supercoolings, whereas the green squares refer to the average growth velocity obtained from SpN at deep supercoolings. The green and red dashed lines correspond to fittings and extrapolations of $v(T)$ using Eqs. (5)–(8) with the "Normal" growth mode. The red and blue symbols refer to the growth velocities of seeds with radii $r = 11$ and 17 A$^{\circ}$, respectively, at temperatures below their onset temperature, T_{on}.

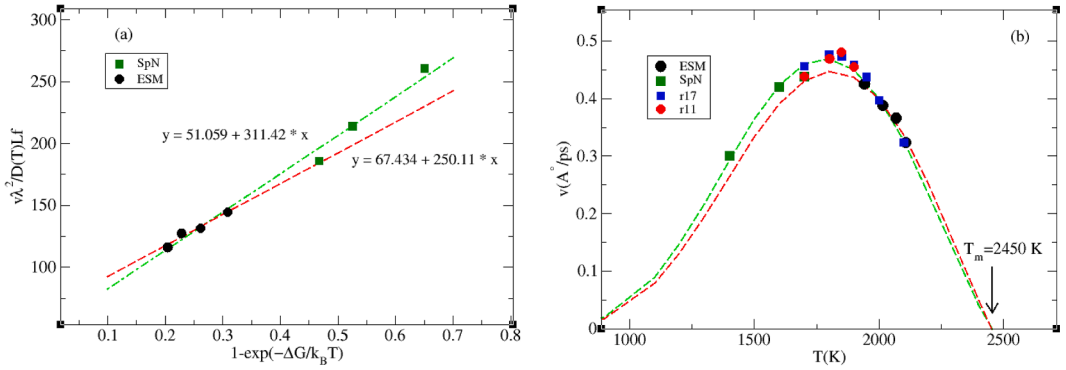

Fig. 8. (a) Reduced growth rates as described in the text (Eq. (9)) considering the "Screw Dislocation" mode of growth, $f << 1$. (b) Temperature dependence of the average crystal growth velocities. The data points are explained in the caption of Fig. 7. The green and red dashed lines refer to fittings and extrapolations of $v(T)$ using Eqs. (5) and (8) with the "Screw Dislocation" growth model.

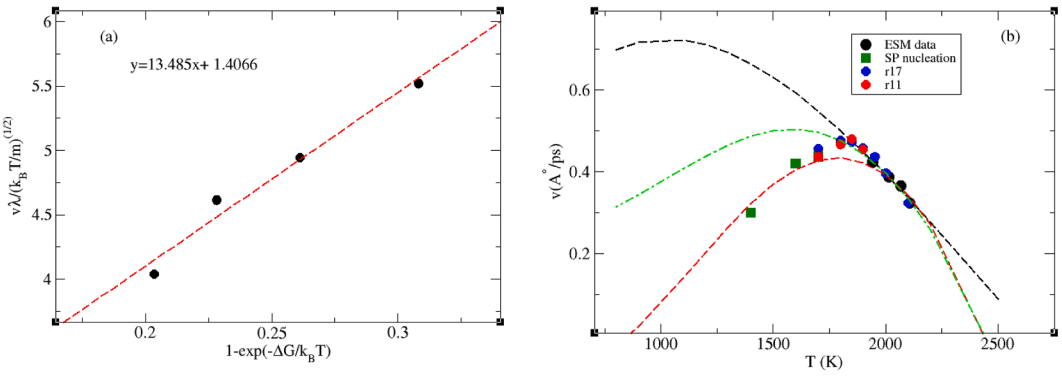

Fig. 9. (a) Reduced growth velocity *vs*. thermodynamic term obtained from Eq. (11). The red line shows the linear fit. (b) Temperature dependence of the average crystal growth velocities in supercooled BaS. Details of the data points were given in the caption of Fig. 7. The dashed lines refer to fittings and extrapolations of $v(T)$ using Eqs. (5) and (11) with both normal (black dashed line) and the "Screw Dislocation" growth model (green and red dashed lines).

mode of growth, with the difference that we considered the temperature dependency of the parameter f. The results of the fits are shown in Fig. 8 (a) and (b). A comparison between Figs. 7 (b) and 8 (b) reveals that the DLT using the screw dislocation mode of growth describes the temperature dependency of the growth rates more accurately. Here we add data obtained from growing a seed with a given size at temperatures lower than its onset temperature, as described in Section 2.3. These data are represented by the red and blue circles in Fig. 7 (b) and 8 (b). As can be observed, the DLT using the screw dislocation mode of growth, accommodates these data points and predicts the melting point obtained in our previous work using the two-phase coexistence method [21].

As mentioned in the Introduction, a maximum in $v(T)$ is often observed in experiments [22], which is a consequence of the competition between the opposing thermodynamic and kinetic dependence on temperature. For most substances, this maximum occurs in a temperature range between the melting point and the glass transition: at $(0.90-0.98)T_m$ for oxide glass-formers and at $(0.6-0.8)T_m$ for metals [66]. Figs. 7 (b) and 8 (b) show that the maximum predicted by the DLT occurs around $T_{v_{max}} = 0.73\ T_m$, which is above the BaS glass transition temperature, $T_g = 0.5T_m$ [59] for the particular cooling rate used here. For a diversity of glass-forming systems: $\frac{T_{v_{max}}}{T_g} = 1.48 \pm 0.15$ [67]. For BaS, this value is quite close: $\frac{T_{v_{max}}}{T_g} = 1.54 \pm 0.02$.

3.2. Prediction of the Collision-Limited Theory (CLT)

According to the CLT [33], the kinetic coefficient is governed by the thermal velocity of particles as

$$k^{CLT}(T) = \frac{fCL}{\lambda}\sqrt{\frac{3k_BT}{m}}, \tag{10}$$

where, m is the particle mass. Using Eqs. (5) and (10), in the framework of the CLT, the rescaled velocity is

$$\frac{\lambda v(T)}{Lf\sqrt{\frac{3k_BT}{m}}} = C[1 - exp(-\Delta G / k_BT)]. \tag{11}$$

Fig. 9(a) shows the rescaled velocity *vs*. $[1 - exp(-\Delta G/k_BT)]$ considering $f \approx 1$. The linear relation shows that this setting is also able to describe the growth rates obtained from the seeding method at shallow supercooling. A linear fit to the data provides the factor C. The value of C, obtained from the slope in Fig. 9(a), is 13.485. Having determined C, we extrapolated the expression to account for deep supercooling, as indicated by the black dashed line in Fig. 9(b). At shallow supercooling or small driving force, there seems to be no significant difference between the DLT and CLT expressions. This is consistent with previous findings from studies on the crystal growth mechanism in the ZnSe semiconductor [20]. However, the distinction between these two theoretical models becomes more pronounce at deeper supercooling. As illustrated in Fig. 9(b), the growth velocity predicted by this theory increases monotonically up to $T_{v_{max}} = 0.45\ T_m$ (black dashed line), which is less than $T_g = 0.5\ T_m$. Considering the temperature dependence of parameter f, we carried out the same procedure using the MD-data obtained from: (i) seeding method (Fig. 9(b), green dashed line) and (ii) both seeding and SpN data points (Fig. 9(b), red dashed line). The fit lines based on the CLT do not align with the MD-derived data obtained from SpN or the data obtained in Section 2.3, shown by red and blue circles.

3.3. Phase field model

The PF model is used as a theoretical and computational tool to predict the evolution of arbitrary morphologies and complex microstructures in materials. In this method, the solid/liquid interface is not sharp and has a finite width. Physical quantities, such as density (referred to as phase fields or order parameters, φ), gradually vary across the liquid/crystal interface [43]. In this approach, the Gibbs free energy is a function of both φ and its gradient $\frac{d\varphi}{dt}$. A traditional PF model based on the hypothesis of local thermodynamic equilibrium, $\frac{\partial\varphi}{\partial t} = 0$, only predicted the linear behavior of $v(T)$ at a small driving force, and was successfully tested by atomistic simulations at a relatively low interface velocity [44]. However, experimental results show that large driving forces can be reached in laboratory, leading to fast solidification rates $\geq$ 10m/s [68]. Diffusion speeds in metallic alloys and semiconductor-based alloys are in the $1-10$ m/s and $0.01-0.1$ m/s ranges, respectively. Galenko et al. [48] recently reformulated the kinetic PF model relying on the fact that the solid/liquid interface may have velocities of the order as, or even exceeding, the diffusion speed in bulk phases [45]. This suggests the transformation will be diffusionless, which introduces nonlinearity in the behavior of crystal growth velocity as a function of undercooling. They considered deviations from local equilibrium in growth kinetics of crystals and adjusted the PF equations to include the first and second derivatives of the order parameter with respect to time. As a result, they derived the associated kinetics equations, proposed a traveling wave solution for these equations, and accounted for nonlinearities in the crystal growth kinetics. Based on their formalism, the interface velocity in the steady-state regime, as a function of undercooling (ΔT), is described as

$$v = \frac{D_\phi(\Delta T)\Delta G(\Delta T)}{\gamma\sqrt{1 + \left[D_\phi(\Delta T)\Delta G(\Delta T)/\gamma v_\phi\right]^2}} \tag{12}$$

and is limited by a maximum speed

$$v_\phi = \sqrt{D_\phi(\Delta T)/\tau_\phi} \tag{13}$$

Table 3
Properties of BaS used to calculate the traveling wave velocity of the phase field.

T_m(K)	γ $(J.m^{-2})$	ΔH_m $(J.m^{-2})$	$D_{0\phi}(m^2/s)$	τ_ϕ (s)	T_A(K)	$E_A/k_B(K)$
2450	0.157	4.74×10^{10}	0.00003527	4.818×10^{-7}	1200	250.61645

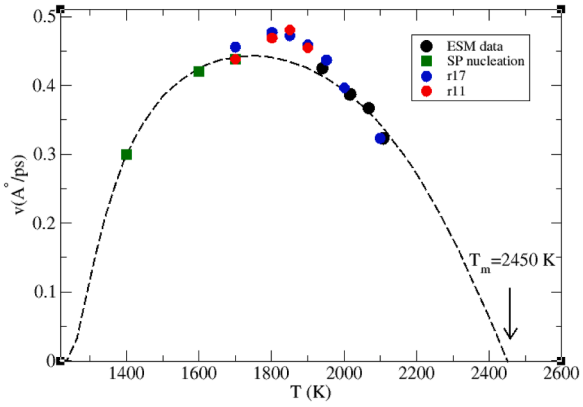

Fig. 10. Average crystal growth velocities in supercooled BaS obatined by the ESM (black circles) and SpN (green squares) *vs.* interface temperature, and fitted curve based on the PF formalism. Details of the data points were given in the caption of Fig. 7.

Here, D_ϕ is the diffusion coefficient of the PF, γ is the interfacial free energy, τ_ϕ is the relaxation time of gradient flow, which is taken as a constant and independent of temperature. D_ϕ is given by

$$D_\phi = D_\phi^0 \exp\left(\frac{-\frac{E_A}{k_B}}{T_m - T_A - \Delta T}\right) \tag{14}$$

where, D_ϕ^0, the diffusion factor of the PF, the energetic barrier, $\frac{E_A}{k_B}$, the pseudo-glass temperature T_A, and τ_ϕ, are obtained from fitting. Fitting the data required previous knowledge of some material properties, such as T_m, γ, and heat of melting, which were determined in a previous work by our research group [51]. The values of the fitting parameters are presented in Table 3. Fig. 10 shows the PF model's fit over the MD-derived data points. The PF model accurately fits the ESM and SpN data points. This model seems to agree with the DLT when assuming a screw dislocation mode of growth. However, its accuracy is called into question when we add the data obtained from growing a seed with a given size at temperatures lower than its onset temperature, as described in Section 2.3. These data are represented by the red and blue circles in Fig. 10.

We also investigated indirectly the nature of the interface between the crystal and the SCL based on Jackson's criterion [64]. This criterion indicates that when the ratio of the crystal melting entropy (ΔS_m) to the melting temperature (T_m) is less than 2 times the gas constant (R), the crystal/liquid interface tends to be rough on an atomic scale ($f \sim 1$), facilitating atomic capture by the growing crystal and layer initiation. Conversely, an interface with ΔS_m exceeding $2R$ might be smoother but potentially have some screw dislocations. For BaS, ΔS_m falls around 1.2×10^{-4}, which is close to $2R$ (1.7×10^{-4}). Consequently, solely based on Jackson's criterion, we cannot definitively conclude whether the BaS interface is rough or smooth.

Although visualizing screw dislocations in growing crystals using programs like OVITO and VMD was not possible, calculating the Burgers vector [69], (beyond the scope of this study) could potentially confirm their presence. However, based on the comprehensive analysis of crystal growth dynamics and the remarkable agreement between our MD simulations and actual growth rates across a range of temperatures, we propose that a screw dislocation mediated growth mechanism best explains the observed behavior. While not a universal phenomenon, screw dislocation growth is a frequently observed mechanism, and in our case, it provides the most convincing explanation for the dynamics observed a posteriori.

4. Summary and conclusions

We investigated crystal growth in supercooled BaS by molecular dynamics simulations. The crystal growth velocities were obtained in a wide temperature range between the melting point and the glass transition temperature, $T = 1400 - 2100$ K. At shallow supercooling, we used the embedded-seed method and estimated the growth velocities of four seed sizes with radii $r^* = 17, 15, 13,$ and 11 A° at their onset temperatures $T_{on} \sim 2114, 2072, 2019,$ and 1945, respectively. At deep supercooling levels, where spontaneous nucleation could be detected, we computed the growth rates directly from time evolution of the number of solid-like atoms at three temperatures $T = 1700, 1600$ and 1400K. The crucial question was: which model, if any, accurately describes the crystal growth rates for different substances across a wide temperature range?

The results indicate that in the high temperature regime, the growth velocity increases linearly as temperature decreases. At deep undercooling, $v(T)$ reaches a maximum. This peak is a well-known characteristic of growth velocity curves that has been observed experimentally and through simulations in other systems. For BaS, this peak occurs at $0.73T_m$, which is significantly higher than its estimated glass transition temperature, $T_g = 0.5\ T_m$, for the studied cooling rate, 50K/ps [59].

Three different models (DLT, CLT, and kinetic PF) were evaluated against the MD-derived data to determine which one describes the BaS crystal growth velocities most accurately. Both the CLT, regarding the temperature dependence of the factor f in Eq. (8), and the kinetic PF model fit the MD-derived data well; however, they failed to accurately capture the maximum velocity and also misrepresented additional velocities obtained from other procedures, as outlined in Section 2.3. The results reveal that the DLT, with the Screw Dislocation mode of growth, best fits the MD data. This model also accurately captured the temperature of the maximum. Moreover, extrapolation *via* the DLT predicts the melting point of BaS, agreeing well with the T_m independently determined using the two-phase coexistence method.

Data availability

All the data used in this study can be made available to any interested reader upon request to the authors.

Declaration of competing interest

We have no conflict of interest regarding the results of this paper.

Acknowledgments

We would like to thank CNPq, Brazil, and the São Paulo Research Foundation, FAPESP, Brazil (contract Cepid no. 2013/007793-6) for funding this study, and the postdoctoral fellowship to LS (grant no. 2019/09499-4).

Appendix

A: Tuning the thermostat relaxation time

Tuning the coupling parameter of the thermostat in the growth simulations is very important and its selection could potentially impact growth velocities, particularly when it is excessively high. During our earlier study in calculations of equilibrium properties of this system, such as density, vibrational density of states, heat capacity as a function of temperature, melting and recrystallization, and structural phase transformation induced by pressure reported in Ref. [21], the thermostat and barostat relaxation times were set to 0.1 and 0.5, respectively, allowing the temperature and pressure to relax every 100- and 500-time steps, respectively, with each time step being 0.001 ps. Because crystallization is an exothermic process, using the same thermostate relaxation time led to a temperature spike at the solid/SCL interface as shown in Fig. A. This figure shows temperature spike coinciding with seed growth due to the released latent heat during crystallization when the thermostat relaxation time was set to 0.1. The same behavior was observed during spontaneous nucleation. The maximum interface temperature obtained from MD is $\Delta T_{in} \sim 5$K related to the growth of seed with radius $r^* = 11\text{A}^\circ$. In this situation we should take into account this spike by increasing the thermostat set temperature with this amount of spike, i.e. $T_{on} = T_{thermostat} + spike = 1945$ K. Otherwise, we should change the thermostat relaxation time to remove this spike, as we have done in our study by setting the thermostat relaxation time to 0.01. Decreasing the thermostat relaxation time (T_{damp}) from 0.1 to 0.005 significantly reduces the temperature spike, as illustrated in Fig. B. It should be emphasized that in our system, because the temperature spike was small, ~ 5 K, changing the T_{damp} was the best way to remove it, whereas in systems with higher temperature spike values, such as 20 K as reported by Monke et al. in their study on the growth mechanism in pure Ni [70], such spikes can significantly affect kinetic coefficients and growth velocities. They attempted to remove this by applying layered thermostat method.

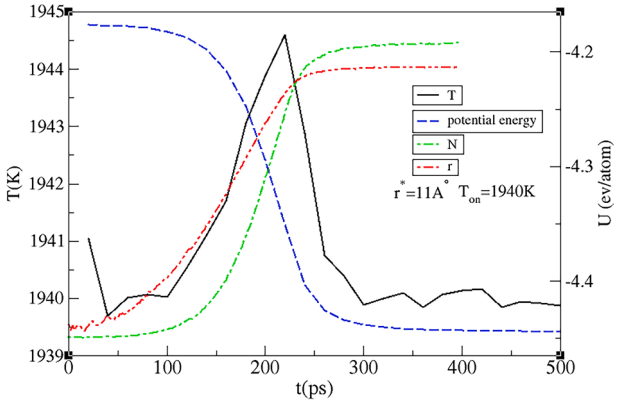

Fig. A. Temperature spike coinciding with seed growth when the thermostat relaxation time was set to 0.1.

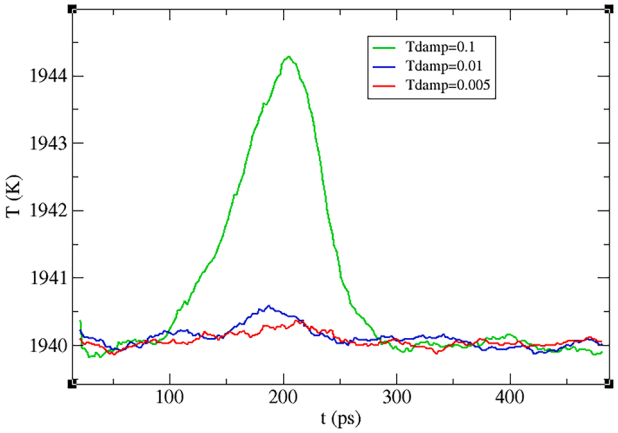

Fig. B. Reducing the temperature spike by decreasing the thermostat relaxation time (T_{damp}) from 0.1 to 0.005.

B: Comparison of atomic flux on the crystal interface and the structural relaxation time

Fig. C shows the relationship between SCL relaxation and crystal growth kinetics in BaS. The times of atomic flux on the crystal interface (average time to grow one atomic layer, $\langle t \rangle$), were calculated using the growth velocities obtained from our MD simulations that are reported in Table 2, and the equation:

$$\langle t \rangle = \lambda / v(T),$$

where, $\lambda = 3.1\text{A}^\circ$ is the jump distance, which is related to the position of the first peak of the radial distribution function of the Ba-S pairs. The structural relaxation times reported in our previous work utilizing the same interaction potential [71], were obtained from the intermediate scattering function:

$$F_s(q,t) = F_s(q)\exp\left[-\left(\frac{t}{\tau_\alpha}\right)^{\beta}\right],$$

where, τ_α is the characteristic structural relaxation time, and β is the stretched exponent. They were obtained as fitting parameters to a F_s versus time plot. The average relaxation time, $\tau_R(T)$, is related to the characteristic relaxation time as follows:

$$\tau_R\ (T) = \frac{\tau_\alpha(T)}{\beta(T)}\Gamma\left(\frac{1}{\beta(T)}\right),$$

where, Γ is the gamma function, $\tau_\alpha(T) = (<\tau_{\alpha,Ba}> + \langle\tau_{\alpha,S}\rangle)/2$ and $\beta(T) = (<\beta_{Ba}> + \langle\beta_S\rangle)/2$. By comparing the relaxation times from our earlier study with the reported growth step times in this work, we found that SCL relaxation significantly precedes crystal growth. This observation demonstrates that SCL relaxation does not directly influence the crystal growth dynamics in BaS in the focused temperature range.

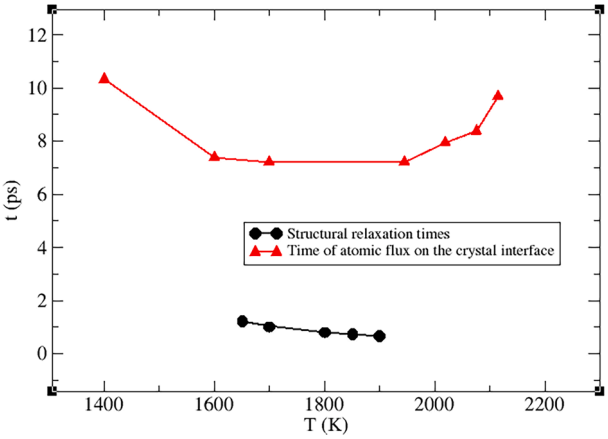

Fig. C. Average structural relaxation time (black) versus average time step for growth (red).

References

[1] D. Turnbull, R.E. Cech, Microscopic observation of the solidification of small metal droplets, J. Appl. Phys. 21 (8) (1950) 804–810.
[2] X.M. Bai, M. Li, Calculation of solid-liquid interfacial free energy: a classical nucleation theory based approach, J. Chem. Phys. 124 (12) (2006) 124707–124719.
[3] J.K. Bording, J. Taft, Molecular-dynamics simulation of growth of nanocrystals in an amorphous matrix, Phys. Rev. B 62 (12) (2000) 8098–8103.
[4] R. Hashimoto, Y. Shibuta, T. Suzuki, Estimation of solid-liquid interfacial energy from Gibbs-Thomson effect: a molecular dynamics study, Isij. Int. 51 (10) (2011) 1664–1667.
[5] J.R. Espinosa, C. Vega, C. Valeriani, E. Sanz, The crystal-fluid interfacial free energy and nucleation rate of NaCl from different simulation methods, J. Chem. Phys. 142 (19) (2015) 194709–194721.
[6] P.K. Bommineni, S.N. Punnathanam, Molecular simulation of homogeneous crystal nucleation of AB2 solid phase from a binary hard sphere mixture, J. Chem. Phys. 147 (6) (2017) 064504–064514.
[7] R.G. Pereyra, I. Szleifer, M.A. Carignano, Temperature dependence of ice critical nucleus size, J. Chem. Phys. 135 (3) (2011) 034508–034513.
[8] D. Suh, K. Yasuoka, Condensation on nanorods by molecular dynamics, J. Chem. Phys. 144 (24) (2016) 244702–244709.
[9] D. Suh, K. Yasuoka, Nanoparticle growth analysis by molecular dynamics: spherical seed, J. Phys. Chem. B 115 (36) (2011) 10631–10645.
[10] D. Suh, K. Yasuoka, Nanoparticle growth analysis by molecular dynamics: cubic seed, J. Phys. Chem. B 116 (50) (2012) 14637–14649.
[11] L. Separdar, J.P. Rino, E.D. Zanotto, Molecular dynamics simulations of spontaneous and seeded nucleation and theoretical calculations for zinc selenide, Comput. Mater. Sci. 187 (2021) 110124.
[12] E. Sanz, C. Vega, J.R. Espinosa, R. Caballero-Bernal, J. Abascal, C. Valeriani, Homogeneous ice nucleation at moderate supercooling from molecular simulation, J. Am. Chem. Soc. 135 (40) (2013) 15008–15017.
[13] P. Montero de Hijes, J.R. Espinosa, C. Vega, E. Sanz, Ice growth rate: temperature dependence and effect of heat dissipation, J. Chem. Phys. 151 (2019) 044509.
[14] K.A. Jackson, The interface kinetics of crystal growth processes, Inter. Sci. 10 (2002) 159.
[15] Y. Ashkenazy, R.S. Averback, Kinetic stages in the crystallization of deeply undercooled body-centered-cubic and face-centered-cubic metals, Acta Mater. 58 (2010) 524.
[16] S. von Alfthan, A.P. Sutton, A. Kuronen, K. Kaski, Stability and crystallization of amorphous clusters in crystalline Si, J. Phys. Condens. Matter 17 (2005) 4263.
[17] Y. Q.Wu, T. Shen, X.M. Lu, N. Zhang, L.S. Lai, S. Gao, Solidification of liquid Fe with embedded homogeneous solid Fe nanoparticles from molecular dynamics simulations, Acta Physico-Chimica Sinica 29 (2013) 245–249.
[18] A. Mattoni, L. Colombo, Non-uniform growth of embedded silicon nanocrystals in an amorphous matrix, Phys. Rev. Lett. 99 (2007) 205501.
[19] T. Zhou, Y. Wu, J. You, The embedded-seed-method molecular dynamics simulation of the crystallization of Al and the influence of the artificial initial stress, J. Cryst. Growth 601 (2023) 126928.
[20] L. Separdar, J.P. Rino, E.D. Zanotto, Decoding crystal growth kinetics and structural evolution in supercooled ZnSe by molecular dynamics simulation, Comput. Mater. Sci. 212 (2022) 111598.
[21] J.P. Rino, An interaction potential for barium sulfide: a molecular dynamics study, Comput. Mater. Sci. 92 (2014) 334–342.
[22] W.L. Chan, R.S. Averback, D.G. Cahill, Y. Ashkenazy, Solidification velocities in deeply undercooled silver, Phys. Rev. Lett. 102 (2009) 095701.
[23] M. Amini, B.B. Laird, Kinetic coefficient for hard-sphere crystal growth from the melt, Phys. Rev. Lett. 97 (2006) 216102.
[24] K.A. Wu, C.H. Wang, J.J. Hoyt, A. Karma, Ginzburge-Landau theory of the bcc-liquid interface kinetic coefficient, Phys. Rev. B 91 (2015) 014107.
[25] K.F. Kelton, Crystal nucleation in liquids and glasses, Solid State Phys. 45 (1991) 75.
[26] H.A. Wilson, On the velocity of solidification and viscosity of super-cooled liquids, Philos. Mag. 50 (1900) 238.
[27] J. Frenkel, On the electric and photoelectric properties of contacts between a metal and a semiconductor, Phys. Z. Sowjetunion 1 (1932) 498.
[28] V.M. Fokin, M.L.F. Nascimento, E.D. Zanotto, Correlation between maximum crystal growth rate and glass transition temperature of silicate glasses, J. Non-Cryst. Solids 351 (2005) 789.
[29] M.L.F. Nascimento, E.D. Zanotto, Mechanism and dynamics of crystal growth, viscous flow, and self-diffusion in silica glass, Phys. Rev. B 73 (2006) 024209.
[30] G.M. Poletaev, Yu V. Bebikhov, A.S. Semenov, R. Yu Rakitin, Molecular dynamics study of the influence of supercooling temperature and orientation of the crystallization front on its velocity in silver, J. Phys. Conf. Ser. 2131 (2021) 042053.
[31] C. Tang, P. Harrowell, Anomalously slow crystal growth of the glass-forming alloy CuZr, Nat. Mater. 12 (2013) 507.
[32] S. An, Y. Li, J. Li, S. Zhao, B. Liu, P. Guan, The linear relationship between diffusivity and crystallization kinetics in a deeply supercooled liquid Ni50Ti50 alloy, Acta Mater. 152 (2018) 1.
[33] J.Q. Broughton, G.H. Gilmer, K.A. Jackson, Crystallization rates of a Lennard-Jones liquid, Phys. Rev. Lett. 49 (1982) 1496.
[34] Q. Gao, J. Ai, Fast crystal growth at ultra-low temperatures, Nat. Mater. 20 (2021) 1431.

[35] C.J. Tymczak, J.R. Ray, Asymmetric crystallization and melting kinetics in sodium a molecular-dynamics study, Phys. Rev. Lett. 64 (11) (1990) 1278.
[36] T. Fang, L. Wang, Y. Qi, Molecular dynamics simulation of crystal growth of undercooled liquid Co, Phys. B 423 (2013) 6.
[37] J.J. Hoyt, B. Sadigh, M. Asta, S.M. Foiles, Atomistic simulation methods for computing the kinetic coefficient in solid-liquid systems, Acta Mater. 47 (1999) 3181.
[38] T. Fang, L. Wang, Y. Qi, Solid-liquid interface growth of Cu50Ni50 under deep undercoolings, Phys. Chem. Liquids 52 (2013) 342.
[39] R. Ramakrishnan, R. Sankarasubramanian, Crystal-melt kinetic coefficients of Ni3Al, Acta Mater. 127 (2017) 25.
[40] X.Q. Yan, Y.J. Lu, Mechanism of abnormally slow crystal growth of CuZr alloy, J. Chem. Phys. 143 (2015) 164503.
[41] Q. Yang, H. Liu, H. Peng, Crystal growth in deeply undercooled Ni50Al50: signature of the ordering sequence at the interface, Chem. Phys. 154 (2021) 194503.
[42] A. Schottelius, et al., Crystal growth rates in supercooled atomic liquid mixtures, Nat. Mater. 19 (2020) 512.
[43] I. Singer-Loginova, H.M. Singer, The phase field technique for modeling multiphase materials, Rep. Prog. Phys. 71 (2008) 106501.
[44] M. Berghoff, M. Selzer, B. Nestler, Phase-field simulations at the atomistic scale in comparison to molecular dynamics, Sci. World J. 2013 (2013) 564272.
[45] D.M. Herlach, P.K. Galenko, D. Holland-Moritz, Metastable Solids from Undercooled Melts, Elsevier, 2007. Amsterdam.
[46] P.K. Galenko, D. Jou, Diffuse-interface model for rapid phase transformations in nonequilibrium systems, Phys. Rev. E 71 (2005) 046125.
[47] P.K. Galenko, D. Danilov, V. Lebedev, Phase-field-crystal and Swift-Hohenberg equations with fast dynamics, Phys. Rev. E (2009) 79.
[48] P.K. Galenko, V. Ankudinov, Local non-equilibrium effect on the growth kinetics of crystals, Acta Mater. 168 (2019) 203–209.
[49] P.K. Galenko, R. Wonnerberger, S. Koch, V. Ankudinov, E.V. Kharanzhevskiy, M. Rettenmayr, Bell-shaped dendrite velocity-undercooling relationship with abrupt drop of solidification kinetics in glass forming Cu-Zr (-Ni) melts, J. Crystal Growth 532 (2020) 125411.
[50] E.T. Karim, M. He, A. Salhoumi, L.V. Zhigilei, P.K. Galenko, Kinetics of solid–liquid interface motion in molecular dynamics and phase-field models: crystallization of chromium and silicon, Philos. Trans. R. Soc. A 379 (2205) (2021) 20200320.
[51] L. Separdar, J.P. Rino, E.D. Zanotto, Unveiling nucleation dynamics by seeded and spontaneous crystallization in supercooled liquids, Comput. Mater. Sci. 199 (2021) 110802.
[52] A.F. Holleman, E. Wiberg, N. Wiberg, Inorganic Chemistry, Academic Press, 2001. San Diego.
[53] S.J. Plimpton, Fast parallel algorithms for short-range molecular dynamics, Comput. Phys. 117 (1995) 1–43.
[54] Y. Sun, H. Song, F. Zhang, L. Yang, Z. Ye, M.I. Mendelev, C.-Z. Wang, K.-M. Ho, Overcoming the time limitation in molecular dynamics simulation of crystal nucleation: a persistent-embryo approach, Phys. Rev. Lett. 120 (2018) 085703–085708.
[55] J. Schindelin, I. Arganda-Carreras, E. Frise, V. Kaynig, M. Longair, T. Pietzsch, S. Preibisch, C. Rueden, S. Saalfeld, B. Schmid, J.Y. Tinevez, D.J. White, V. Hartenstein, K. Eliceiri, P. Tomancak, A. Cardona, Fiji: an open-source platform for biological-image analysis, Nat. Methods 9 (2012) 676.
[56] P.J. Steinhardt, D.R. Nelson, M. Ronchetti, Bond-orientational order in liquids and glasses, Phys. Rev. B 28 (1983) 784.
[57] P.R. ten Wolde, D. Frenkel, Homogeneous nucleation and the Ostwald step rule, Chem. Phys. 1 (1999) 2191.
[58] J.R. Espinosa, C. Vega, C. Valeriani, E. Sanz, Seeding approach to crystal nucleation, J. Chem. Phys. 144 (2016) 034501–034510.
[59] S.C.C. Prado, J.P. Rino, E.D. Zanotto, Successful test of the classical nucleation theory by molecular dynamic simulations of BaS, Comp. Mat. Sci. 161 (2019) 99–106.
[60] I. Gutzow, E. Kaldis, H.J. Scheel, Crystal Growth and Materials, North-Holland Publ. Comp., Amsterdam - New York, (1977) (Ed.) 1977, pp. 379–414 Chap. 1.11.
[61] D. Kashchiev, Nucleation: Basic Theory With Applications, Butterworth-Heinemann, 2000. Oxford.
[62] (Ed.) K.A. Jackson, R.H. Doremus, B.W. Roberts, D. Turnbull, Growth and Perfection of Crystals, Wiley, 1958 (Ed.)New York.
[63] W.K. Burton, N. Cabrera, F.C. Frank, The growth of crystals and the equilibrium structure of their surfaces, Proc. R. Soc. Lond. A 243 (1951) 299.
[64] D.R. Uhlmann, Crystal growth in glass-forming systems: a ten-year perspective, nucleation and crystallization in glasses, Adv. Ceram. Am. Ceram. Soc. 20 (1982) 20.
[65] L.L. Burgner, M.C. Weinberg, Crystal growth mechanisms in inorganic glasses, Phys. Chem. Glasses 42 (2001) 184.
[66] J. Jiusti, E.D. Zanotto, D.R. Cassar, M.R.B. Andreeta, Viscosity and liquidus-based predictor of glass-forming ability of oxide glasses, J. Am. Ceram. Soci. 103 (2020) 921.
[67] J. Ovrava, L. Greer, Fast and slow growth kinetics in glass-forming melts, J. Chem. Phys. 140 (2014) 214504.
[68] E.J. Lavernia, T.S. Srivatsan, The rapid solidification processing of materials: science, principles, technology, advances, and applications, J. Mater. Sci. 45 (2010) 287.
[69] D. Hull, D.J. Bacon, Dislocations in Other Crystal Structures, Butterworth-Heinemann, 2011, pp. 109–136. ISBN 9780080966724.
[70] J. Monk, Y. Yang, M.I. Mendelev, M. Asta, J.J. Hoyt, D.Y. Sun, Determination of the crystal-melt interface kinetic coefficient from molecular dynamics simulations, Model. Simul. Mater. Sci. Eng. 18 (2010) 0150.
[71] J.P. Rino, S.C.C. Prado, E.D. Zanotto, The race between relaxation and nucleation in supercooled liquid and glassy BaS: a molecular dynamics study, J. Chem. Phys. 149 (2018) 024503–024513.